

Separating Attitude and Shape Effects for Non-resolved Objects

Doyle Hall¹, Brandoch Calef², Keith Knox², Mark Bolden³, and Paul Kervin³

¹*Boeing LTS / AMOS, Kihei, HI and Colorado Springs, CO*

²*Boeing LTS / AMOS, Kihei, HI*

³*Air Force Research Laboratory / Detachment 15, Kihei, HI*

1 SUMMARY

Radiometric measurements provide a means of constraining the attitude and/or shape of on-orbit objects that are too small or distant to be imaged by ground-based optical or radar facilities. At the most general level, a detailed analysis of radiometric data to determine attitude and shape entails the numerical inversion of a multivariate integral equation involving two classes of variables: “attitude” and “body” parameters. Attitude parameters specify the object orientation at the times of the observations and provide a means to convert between the inertial reference frame and the body-fixed reference frame. Body or “shape” parameters provide the information required to calculate the radiant intensity of the object from within the body-fixed reference frame. Our analysis indicates that the most basic requirement for the analysis is an extensive set of radiometric observations, ideally gathered from multiple perspectives and under multiple illumination conditions. Given such a rich data set, a complete attitude/shape inversion analysis requires supercomputer resources to address in a timely fashion, even for relatively simple convex objects. The basic reason for this is that the inversion approach requires solving for a large number of object attitude and shape parameters. A significantly more computationally efficient means of addressing the problem would be to separate the attitude and body parameter determination analyses, if at all possible. To this end, we present a variety of theoretical approaches for both shape-independent attitude analysis and attitude-independent shape analysis for non-resolvable objects.

2 INTRODUCTION

Many Earth-orbiting satellites are too small or distant to be imaged by even the most advanced ground-based optical and radar instrumentation. This non-resolvable population includes many geo-synchronous satellites, and a quickly growing number of micro- and nano-satellites. Notably, the capabilities of even the smallest 10 cm-sized pico-satellites have become surprisingly sophisticated during the last decade. Determining the size, shape, and attitude (i.e., orientation) of any unknown satellite is an essential first step in evaluating the payload function and capability. Fortunately, non-imaging optical observations provide a means of constraining these essential satellite characteristics. In this regard, time-resolved photometry and radiometry are of particular interest because such data can be gathered relatively easily and because the asteroid observation community has developed methods capable of determining both the shapes [1, 2, 3] and spin-state attitudes [1, 4] of non-resolvable asteroids.

While some of the methods developed by the asteroid community can be applied to Earth-orbiting satellites, characterizing man-made objects requires many different theoretical considerations. For instance, asteroids have nearly smooth and uniform powdery surfaces that reflect sunlight in a predominantly diffuse fashion [1, 2], whereas man-made satellites have highly angular shapes covered by a variety of materials that are often very shiny. Also, asteroids generally spin in a stable fashion and their attitude can be modeled using relatively simple spin-state rotational equations of motion [1, 4]. The attitudes of Earth-orbiting satellites vary dramatically and generally require much more detailed mathematical or computational models. For instance, complex active attitude control systems maintain the orientation of stabilized satellites. Even uncontrolled satellites are subject to dynamic on-orbit torque perturbations, and generally would be expected to occupy rotation states more complicated than stable spins.

These complications indicate that deriving detailed information about attitude and shape for man-made satellites requires a more general theoretical framework than that used by asteroid astronomers. During the past few years, AMOS researchers have begun to assemble such a framework, and have outlined the

problem in mathematical terms. The analysis can be formulated as a numerical integral-equation inversion problem, where observational data are inverted to determine estimates for satellite attitude and body parameters. The most basic requirement for such an inversion analysis is an extensive set of radiometric observations, ideally gathered from multiple perspectives and under multiple illumination conditions. However, given a sufficient input data set, performing a complete inversion analysis to determine both attitude and body parameters requires extensive computation, even for convex objects. This arises for two reasons. First, describing a satellite's shape and reflectance/emittance characteristics to a sufficient level of detail can require a very large number of body parameters. Second, describing a satellite's attitude throughout an observation period requires a set of highly non-linear parameters that generally do not lend themselves to efficient computational determination.

One way of addressing the computational requirements is to formulate the mathematical equations in a manner that separates the attitude and body parameters as much as possible, and clearly identifies parts that depend on each. This effort breaks up the multivariate inversion problem into a set of restricted problems with smaller dimensionality, subdivided naturally into independent parts that can be calculated in parallel on a multi-node computer. Another strategy is to try to formulate analysis methods that are completely independent of either the attitude or body parameters. In this regard two basic strategies can be pursued: *attitude-independent shape analysis* and/or *shape-independent attitude analysis*.

3 ATTITUDE AND SHAPE INVERSION THEORY

A basic understanding of the theory of inverting time-resolved non-imaging observations to determine attitude and shape can be gained by studying the simplified illustrative case of an idealized single photometric sensor observing a satellite reflecting sunlight. For this discussion, the satellite is idealized as a rigid body with unchanging surface reflectivity parameters. (Note, the restrictive assumptions made here for purposes of simplified theoretical illustration can be relaxed in more generalized treatments of multi-site and multi-sensor observations of flexible or articulating satellites with concavities as well as reflectance properties that change under the influence of space weathering.) In this idealized case, the sensor would yield a measure of the radiant intensity of reflected sunlight, L , integrated over a particular spectral band as a function of time. This radiant intensity (given in units of $W\ ster^{-1}$) varies in response to changes in the relative positions of the body, Sun, and observer, as well as changes in the attitude of the satellite. Given a detailed knowledge of the sensor characteristics, the illuminating solar flux, and the satellite trajectory, then the intensity could be calculated using a forward model, but only if one had detailed a priori knowledge of the satellite's attitude as well as its shape and reflectance characteristics. Thus, the radiant intensity can be thought of as depending on two generalized classes of variables in addition to time itself: attitude and body parameters

$$L = L(t, \mathbf{p}_{\text{Attitude}}, \mathbf{p}_{\text{Body}}) \quad (1)$$

3.1 Attitude Parameters

Attitude parameters, $\mathbf{p}_{\text{Attitude}}$, provide all of the information required to describe the object's attitude throughout the observation period. In other words, they provide a means of specifying the orientation of the body in an inertial reference frame (taken here to be the Earth-centered J2000 equatorial frame). For a stably spinning satellite, the attitude parameters would necessarily include the spin rate and spin axis orientation. For a satellite that has an active attitude control system (ACS), more detailed attitude parameters would be required in order to simulate the performance of the ACS hardware and software. Actively slewing satellites, such as Hubble Space Telescope, would require even more parameters (e.g., slew times, slew rates, etc.).

In mathematical terms, $\mathbf{p}_{\text{Attitude}}$ comprises the set of all parameters required to specify the body's "attitude matrix", \mathbf{R} , as a function of time. This 3×3 rotation matrix converts vectors from the inertial reference frame into the body-fixed reference frame, and can be written symbolically as follows:

$$\mathbf{R} = \mathbf{R}(t, \mathbf{p}_{\text{Attitude}}) \quad (2)$$

As an example, the attitude matrix provides the means to convert the time-dependent satellite-to-observer unit direction vector in the inertial reference frame, $\mathbf{o}^*(t)$, into a body-frame vector through matrix multiplication as follows:

$$\mathbf{o}(t, \mathbf{p}_{\text{Attitude}}) = [\mathbf{R}(t, \mathbf{p}_{\text{Attitude}})] [\mathbf{o}^*(t)] \quad (3)$$

In this discussion, the “*” superscript denotes inertial frame vectors and body-frame vectors are denoted without superscripts. The satellite-to-Sun inertial unit direction vector can be similarly written:

$$\mathbf{s}(t, \mathbf{p}_{\text{Attitude}}) = [\mathbf{R}(t, \mathbf{p}_{\text{Attitude}})] [\mathbf{s}^*(t)] \quad (4)$$

The two direction vectors given in Eqs. (3) and (4) play an important role in determining the observed brightness of sunlight reflected from the body, as described below.

3.2 Body Parameters

Body parameters provide information about the shape of the object as well as the reflective properties of its surfaces. In mathematical terms, \mathbf{p}_{Body} comprises the set of all parameters required to calculate the radiant intensity from within the body reference frame. A multi-faceted convex Lambertian reflector provides a simple example of how to define a set of body parameters particularly well suited for describing man-made satellites. This example also illustrates the development of the “albedo-area distribution” which itself can be used as a complete set of body parameters for convex objects.

Highly angular bodies such as man-made satellites are naturally decomposed into a finite set of flat surfaces (i.e., facets). Each facet may be described as a planar polygon. In this example, the k^{th} facet is characterized by a Lambertian reflectance or albedo (a_k), a total area (A_k), and a normal unit vector (\mathbf{n}_k – specified in body-frame coordinates). The radiant intensity of the entire satellite may then be written as a sum of the sunlight reflected from each of the facets:

$$L(t, \mathbf{p}_{\text{Attitude}}, \mathbf{p}_{\text{Body}}) = \sum_k a_k A_k \left[\frac{F_{\text{Sun}}(t) \langle \mathbf{n}_k \cdot \mathbf{o}(t, \mathbf{p}_{\text{Attitude}}) \rangle \langle \mathbf{n}_k \cdot \mathbf{s}(t, \mathbf{p}_{\text{Attitude}}) \rangle}{\pi} \right] \quad (5)$$

where the angular brackets denote the non-negative operator:

$$\langle x \rangle \equiv \begin{cases} x & x \geq 0 \\ 0 & x < 0 \end{cases} \quad (6)$$

Eq. (5) demonstrates the dependence of the radiant intensity on the illuminating solar flux, F_{Sun} (given in units W m^{-2}), and the satellite-to-observer and satellite-to-Sun direction vectors given by Eqs. (3) and (4), respectively. Eq. (5) can be re-written:

$$L(t, \mathbf{p}_{\text{Attitude}}, \mathbf{p}_{\text{Body}}) = \sum_k a_k A_k K(t, \mathbf{n}_k, \mathbf{p}_{\text{Attitude}}) \quad (7)$$

where the kernel function, K , is given in the square brackets in Eq. (5). For objects with round surfaces, the finite summation over facets in Eq. (7) can be expressed as an integral over a distribution of facets:

$$L(t, \mathbf{p}_{\text{Attitude}}, \mathbf{p}_{\text{Body}}) = \int d\boldsymbol{\omega} aA(\boldsymbol{\omega}) K(t, \boldsymbol{\omega}, \mathbf{p}_{\text{Attitude}}) \quad (8)$$

In Eq. (8), the function $aA(\boldsymbol{\omega})$ denotes the “albedo-area distribution” of the body, which specifies the albedo-area product per steradian summed over all facets that lie normal to the body-frame direction $\boldsymbol{\omega}$.

The integration spans all 4π steradians of solid angle and thereby accounts for all possible facet orientations. In cases where the body has no facets at all normal to the ω direction, $aA(\omega)$ equals zero. By simple inspection of Eq. (8) one can see that, in this case, the distribution $aA(\omega)$ specifies the entire set of body parameters.

Similar integral equations apply to thermal-IR observations, in which a convex body can be described by an “emissivity-area (eA) distribution” similar in concept to the aA distribution presented above. Preliminary analysis indicates that fusing visible and thermal-IR observations may provide a means to retrieve the facet area distribution $A(\omega)$ as well as separate estimates of $a(\omega)$ and $e(\omega)$. However, for this discussion only the analysis of reflected sunlight will be considered in detail.

3.3 Inversion Theory and Numerical Implementation

Suppressing the attitude and body parameters in Eq. (8) yields an equation with a very simple and recognizable form

$$L(t) = \int d\omega aA(\omega) K(t, \omega) \quad (9)$$

which is a Fredholm Integral Equation of the First Kind. The kernel function for this integral equation has the notable quality that it maps between the two dimensions of facet-normal angle (ω) and the one dimension of time (t). Finding numerical solutions for such integral equations has been researched in detail, and generally entails the use of matrix factorization or gradient-descent search methods [5, 6]. In practice, these methods provide a means to invert the integral equation and derive a non-negative albedo-area distribution that provides a best-fit to the input data.

More general treatments for bodies that have non-Lambertian bidirectional reflectance distribution functions (BRDFs) also lead to integral equations. For instance, if each facet has a diffuse reflectance (like that given above) plus a specular mirror-like reflectance, then

$$L(t, \mathbf{p}_{\text{Attitude}}, \mathbf{p}_{\text{Body}}) = \int d\omega [aA_D(\omega) K_D(t, \omega, \mathbf{p}_{\text{Attitude}}) + aA_S(\omega) K_S(t, \omega, \mathbf{p}_{\text{Attitude}})] \quad (10)$$

where D and S subscripts denote diffuse and specular components, respectively. The integrand in Eq. (10) comprises a two-term sum, one for each reflectance component. Similarly, accounting for facets composed of different surface materials with known BRDFs (like polished aluminum, white paint, solar array, etc.) entails using a multi-term integrand, with each term corresponding to a different material:

$$L(t, \mathbf{p}_{\text{Attitude}}, \mathbf{p}_{\text{Body}}) = \int d\omega \left[\sum_m aA_m(\omega) K_m(t, \omega, \mathbf{p}_{\text{Attitude}}) \right] \quad (11)$$

where the sum over m spans all possible materials (or, more generally, reflective components).

So far this formulation has treated time, t , as a continuous mathematical variable. However, real satellite observations generally come in the form of discrete measurements, described by the following composite data set:

$$\{t_i, T_i, L_i, \Delta L_i, \mathbf{o}_i^*, \mathbf{s}_i^*\} \quad i = 1 \dots N_{\text{Observations}} \quad (12)$$

where t_i denotes the mid-point time of the i^{th} observation, T_i the exposure duration, L_i the measured radiant intensity, ΔL_i the measurement uncertainty, \mathbf{o}_i^* the inertial frame body-to-observer unit direction vector at the mid-point of the observation, and \mathbf{s}_i^* the body-to-Sun direction vector. In this discussion, we assume for simplicity that exposure durations are sufficiently short to effectively “freeze the action” so that the measurements can be approximated as instantaneous samples. In this case, the observations can be numerically modeled using a discrete form of Eq. (11):

$$L_i(\mathbf{p}_{\text{Attitude}}, \mathbf{p}_{\text{Body}}) = \sum_{k,m} aA_m(\boldsymbol{\omega}_k) K_m(t_i, \boldsymbol{\omega}_k, \mathbf{p}_{\text{Attitude}}) \quad (13)$$

where the set of facet-normal directions $\{\boldsymbol{\omega}_k\}$ comprises a discrete grid that spans all 4π steradians of the unit sphere. Eq. (13) can be simplified by combining the indices k and m into one master index j and rewriting as follows:

$$L_i(\mathbf{p}_{\text{Attitude}}, \mathbf{p}_{\text{Body}}) = \sum_j aA_j K_{i,j}(\mathbf{p}_{\text{Attitude}}) \quad (14)$$

Eq. (14) provides an immediate means of identifying which parts of the inversion equation depend on body and attitude parameters, respectively. Notably, the set of albedo-area products $\{aA_j\}$ serves as a complete set of body parameters. Furthermore, the attitude parameters appear only in the kernel functions. Eq. (14) indicates a system of equations—one equation per observation. The goal of the analysis is to numerically invert this system and thereby calculate the best-fit attitude and body parameters that minimize the least-squares metric:

$$\chi^2(\mathbf{p}_{\text{Attitude}}, \mathbf{p}_{\text{Body}}) = \sum_i \left(\frac{L_i - L_i(\mathbf{p}_{\text{Attitude}}, \mathbf{p}_{\text{Body}})}{\Delta L_i} \right)^2 \quad (15)$$

3.4 Coupled Attitude and Shape Analysis

The formulation presented so far yields an integral-equation inversion problem in which the attitude and body variables are coupled, and must be solved for as a unified set. Because the total number of these parameters can be surprisingly large, even for simple convex objects, this task generally requires extensive computation. One way of mitigating the computational requirements is to break up the multivariate inversion problem into a set of restricted problems with smaller dimensionality. For the current problem, this entails solving for the body parameters *for a given set of attitude parameters*. Repeating this process provides a means of investigating many different sets of attitude parameters to determine which ultimately yields the best fit to the data. Because each calculation is independent of the others, this process naturally lends itself to parallel computation on a multi-node computer.

Preliminary analysis indicates that this method holds special promise for stabilized satellites, because the number of commonly-employed ACS modes is relatively small (i.e., a few dozen or so). Thus, if a non-resolvable object is thought to be stabilized, then inversion analyses to solve for aA distributions could be performed separately for the attitude parameters corresponding to the most common ACS modes. Each inversion should be graded on how well the input data are reproduced via Eq. (15). For the best matches, the aA distributions could be analyzed to search for characteristic object shape properties (as discussed in the next two sections). Similar methods can also be applied to non-stabilized attitudes, such as spinning objects or other rotational states. However, in these cases, inversions must be calculated for a potentially very large number of rotational state parameters in order to evaluate the best match.

Note that, for a given set of attitude parameters, Eq. (14) appears to be a linear system that can be solved simply by inverting the kernel matrix, or by using one of a variety of other linear system numerical solution algorithms [5]. However, this is not the case here, because the aA_j values must be non-negative to make physical sense, and a simple linear system algorithm would likely produce some negative values. Such negative values could result from incomplete sampling, measurement noise, or numerical round-off error. In fact, unstable inversions suffer from “ringing”, where the solution vector contains large-amplitude negative and positive elements that produce a good fit to the data, but are physically implausible. Fortunately, detailed and efficient matrix-factorization algorithms exist for calculating non-negative solutions for such systems [6]. However, for extremely large systems, gradient-descent search methods (see [5, 7] and references therein) may provide a more efficient method of calculation.

3.5 Facet Area Distribution Functions and Body Shapes

More than a century ago, H. Minkowski laid the foundations of a method to reconstruct the shape of a convex object from its facet-area distribution (see [7] and references therein). Unfortunately, single-band visible or thermal-IR observations only yield information on aA or eA product distributions, respectively, whereas shape reconstruction requires the facet-area distribution, $A(\omega)$. As mentioned above, combining visible and thermal-IR observations may provide a means to retrieve $A(\omega)$ as a separated quantity [7]. However, even for single-band observations, one approximation that can be employed is to assume the albedo or emissivity of all facets to be the same and equal to a value representative for a typical satellite surface material. In this case, Minkowski reconstruction would produce an approximate version of the object's shape, which could be distorted if there were significant facet-to-facet a or e variations on the actual satellite.

Even in the absence of a full shape reconstruction, just the properties and symmetry of a derived aA or eA distribution provides significant information about an object's shape. One way to conceptualize this is to imagine the aA distribution resulting from a perfectly successful inversion analysis for a cubical satellite comprised of six identical facets. Figure 1 (left panel) schematically illustrates an aA distribution for this case using a Mollweide projection plot of the distribution as a function of ω . The distribution comprises six "spikes" or delta-functions each at the angular location of the cube's six facet normal vectors and each separated by 90° from the nearest neighbors. In an actual numerical inversion, these spikes would tend to manifest themselves as tight clusters of relatively large aA values. If the cube's facets were not identical but had different albedos, then the six spikes would appear in the same locations on the diagram but with unequal magnitudes. Figure 1 (right panel) illustrates the distribution for a cylinder with the axis of symmetry aligned with the body-frame z-axis. This distribution has spikes at each pole representing the two flat facets at each end of the cylinder, and a continuous arc along the equator representing the round portion. Although not shown in Figure 1, a uniform reflective sphere corresponds to a constant aA product distribution over all facet directions ω .

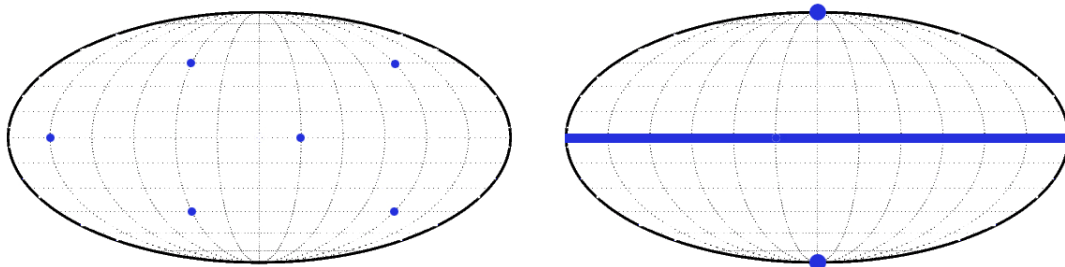


Figure 1. Mollweide projections of the albedo-area product distributions for a cube (left panel) and a cylinder (right panel). The distribution for a perfect cube comprises six delta-functions (represented by the dots) at the angular locations of the six facets. For a cylinder, two delta-functions at the poles represent the flat ends of the cylinder and a continuous distribution along the equator (solid line) represents the round portion.

Figure 1 graphically illustrates how the properties of derived aA or eA distributions can provide shape information. For instance, if the distribution contains a number of statistically significant spikes or tight clusters, then the observed object likely has at least that many flat facets. If the clusters tend to be separated by a characteristic angle from their nearest neighbors, then the corresponding facet normal vectors are also separated by that characteristic angle. As illustrated in Figure 1 (left panel), 90° separations suggest cubical or rectilinear body symmetry. Similarly, hexagonal prisms produce spikes separated by 60° , octagonal prisms produce 45° separations, and so on. Distributions that show statistically significant evidence of continuous arcs in the form of great circles (similar to the equatorial distribution in the right panel of Figure 1) suggest cylindrical symmetry. Conical shapes also produce distributions characterized by continuous arcs. Finally, distributions with large uniform regions suggest bodies with surfaces that are partly or nearly spherical.

3.6 Objects with Concavities

The theory presented so far applies to convex objects. Concavities complicate the situation significantly. For convex objects reflecting sunlight, the aA distribution serves as a complete set of body parameters, and can be calculated using relatively efficient numerical methods. However, concave objects can experience facet-to-facet shadowing and obscuration. This requires the use of self-shadowing and self-obscuration factors in the kernel functions, and calculating these factors requires knowing the *relative positions* of the facets in addition to their aA products. Notably, asteroid astronomers have developed a method of determining asteroid concavities [2]. Unfortunately, that method as implemented appears to be unsuitable for man-made satellites because it relies heavily on the relatively smooth texture and diffuse reflectance properties of asteroids in order to converge to a meaningful result. Further research needs to be conducted on adapting this method to man-made satellites, as well as on formulating generalized body parameters that describe highly angular objects with concavities and identifying appropriate numerical inversion methods.

In the short term, one simple approach is to neglect the influence of the concavities during the analysis and solve for the “best-fit convex model.” The net result of this inversion analysis would likely be a derived aA or eA distribution that fails to reproduce the complete set of observations because the effects of self-shadowing and self-obscuration were neglected. However, even with this deficiency, this approximate distribution could still reveal information about the object’s shape, as discussed above. For instance, distributions that show statistically significant evidence of spikes or tight clusters would still suggest the existence of flat facets. However, in this case these facets could be part of a sub-component of the non-convex body. Similarly, continuous arcs in the distribution suggest the existence of cylindrical/conical symmetry possessed by either the entire body or by sub-components. Finally, large uniform regions in the distribution suggest nearly-spherical surfaces on either the main body or sub-components.

4 SHAPE-INDEPENDENT ATTITUDE ANALYSIS

The previous section discussed a formulation of retrieving attitude and shape parameters as a coupled set, and relied on numerical inversion methods to provide a best fit to the radiant intensity data. However, there are other analysis methods that provide a determination of the object’s attitude, or at least a constraint on the object’s orientation, as discussed below.

4.1 Synodic vs. Sidereal Period Spin State Analysis

Periodic or quasi-periodic modulation of a satellite’s brightness often indicates rotational motion. In the simplest case of a stationary spinning satellite illuminated by a stationary light source and observed by a stationary observer, the period of the brightness modulations corresponds to the spin period. However, if a spinning body moves quickly with respect to an observer, the apparent rotation rate *as seen from the observer’s perspective* can deviate significantly from the actual rotation rate of the body. An extreme example in this respect is the Moon, which always presents the same face to the Earth, showing no apparent rotation to terrestrial observers, even though it actually rotates once every 28 days. Exploiting this effect, asteroid researchers have developed a method for determining spin states of non-resolved objects (see [4, 1] and references therein). The method relies on measuring variations in “synodic” brightness modulation rates in order to determine an object’s “sidereal” spin rate as well as spin axis orientation. The distinction between synodic and sidereal periods has been discussed in detail by the asteroid observational community (see [4, 1] and references therein). Synodic or apparent periods are measured directly from the brightness data. Variations in synodic periods arise from the relative motions of the satellite, observer, and illumination source. In order to evaluate satellite spin states using this method two analyses are required. First, the brightness data must be analyzed to determine accurate synodic modulation periods, typically using Fourier or similar analysis techniques [8, 9, 10]. Second, these synodic periods must be converted to a best-fit sidereal rotation period by accounting for the effects of the relative motion of the satellite, observer, and illumination source during the observations. This latter step requires an analysis to determine the spin axis orientation [10]. Notably, instead of finding a best fit to the observed brightness data directly, this method finds a best fit to the *periodicity* of the brightness modulations. Because this periodicity only depends on the object’s spin rate, the analysis is completely independent of object shape. However, after the spin-state is determined using this method, an albedo-area determination analysis can be performed with this set of attitude parameters to constrain the object’s shape.

Unfortunately, when observing objects from one or more ground-based sites, the synodic/sidereal method can only be realistically applied when three conditions are met: 1) the object is in a stable or slowly changing spin rotation state throughout the observational period, 2) the spin rate is rapid enough so that the resulting modulation periods can be measured accurately during single-pass observations, and 3) the object traverses over the observation sites sufficiently quickly so that the difference between synodic and sidereal periods is measurable. If these conditions are met, this method provides an extremely computationally efficient way to derive the attitude of man-made satellites. For instance, the method was successfully applied to determine the spin state of NASA’s IMAGE satellite to help diagnose its operational status after ceasing transmissions in late 2005 [10]. Research continues to extend the method to more complicated rotation states (e.g., precession, nutation, etc.).

4.2 Glint Analysis

Satellites often glint sunlight, and these events can be used to constrain attitude. For instance, a large flat surface, such as a solar array panel, glints when the angle of incoming sunlight equals (or nearly equals) the outgoing angle towards an observer, i.e., when the “specular condition” for the facet is satisfied. Another way to express this specular condition is that the normal to the facet nearly coincides with the “phase angle bisector” (PAB), which is defined as the unit direction vector midway between the satellite-to-Sun and satellite-to-observer vectors:

$$\mathbf{b}^*(t) \equiv \frac{\mathbf{o}^*(t) + \mathbf{s}^*(t)}{|\mathbf{o}^*(t) + \mathbf{s}^*(t)|} \quad (16)$$

A glint occurring at a time t_G indicates that, at that time, the facet normal and the PAB coincide:

$$\mathbf{n}^*(t_G) \cdot \mathbf{b}^*(t_G) = 1 \quad (17)$$

where $\mathbf{n}^*(t)$ denotes the unit normal to the facet in the inertial reference frame, which varies in time in response to changes in satellite orientation. For most materials, significantly enhanced reflection also occurs when the facet normal and the PAB *nearly* coincide (i.e., when the dot product in Eq. (17) approximates one). Notably, satellite sub-components with other shapes have different specular conditions, which generally can also be conveniently expressed in terms of the PAB. For instance, a cylinder glints when its axis lies perpendicular to the PAB:

$$\mathbf{c}^*(t_G) \cdot \mathbf{b}^*(t_G) = 0 \quad (18)$$

where $\mathbf{c}^*(t)$ denotes the time-dependent unit vector along the cylinder axis.

After a glint is observed, the PAB orientation at the time of the event can be calculated relatively easily using the known positions of the observer, satellite and Sun along with Eq. (16). Furthermore, knowing the orientation of the PAB constrains the orientation of the glinting component through specular conditions like those given in Eqs. (17) and (18). For instance, stabilized geosynchronous and geostationary (GEO) satellites with solar panels that track the Sun tend to glint strongly as the satellites skirt just outside the Earth’s shadow—because at these times the PAB very nearly coincides with the panels’ normal vector, and Eq. (17) is approximately satisfied. In fact, the specific timing of such GEO glint events can even be used to determine or constrain satellite solar panel orientations [11]. Conversely, observing such glints from an unknown GEO satellite is a strong indicator that it possesses panels that track the Sun. Alternatively, observing a sequence of sharp glints of relatively small magnitude from a nano-satellite can indicate that it possesses one or more small cylindrical wire antennas, as many do. The wire orientations can be derived from the known PAB orientations during the glint events via Eq. (18), and an attitude history for the set of antennas can potentially be assembled over time from the observed sequence.

4.3 Single-Facet Orientation Analysis

Occasionally, stabilized or slowly rotating satellites can display a notable brightening or dimming in radiant intensity while making a pass over a terrestrial observer, caused by the change in illumination or visibility of a single large facet. Such signatures can potentially be exploited to determine or constrain the orientation of that surface. For instance, consider a stabilized low-Earth orbit (LEO) satellite that has a large reflective surface that it maintains on its leading side, normal to the velocity vector. This surface will tend to be seen edge-on near the culmination (i.e., the highest point) of passes over ground-based observers. Furthermore, during early phases of the passes the surface will present its full reflective area to observers, and during late phases will be obscured by the satellite body. Such a leading surface can therefore produce signatures that notably dim at or near pass culmination, and this pattern will be repeatable for similar observation geometries. Similarly, a large trailing surface can cause repeatable brightening signatures near pass culminations. Such single-facet signatures can be caused by the surface becoming edge-on to the observer (leading to a change in visibility as in the examples just cited), or by becoming edge-on to incoming sunlight (leading to a change in illumination). Either effect can cause brightening or dimming signatures. Examining the timing and pattern of such signatures can potentially reveal the existence and orientation of large flat surfaces on a satellite. Simulation studies indicate that the method works best for LEO satellites, and the effectiveness greatly enhanced when such signatures can be observed simultaneously from two ground-based sites. For instance, observations from Maui and Kauai can distinguish between LEO single-facet signatures caused by changes in illumination, which occur simultaneously at both sites, versus those caused by changes in visibility, which occur separated in time (see Figure 2).

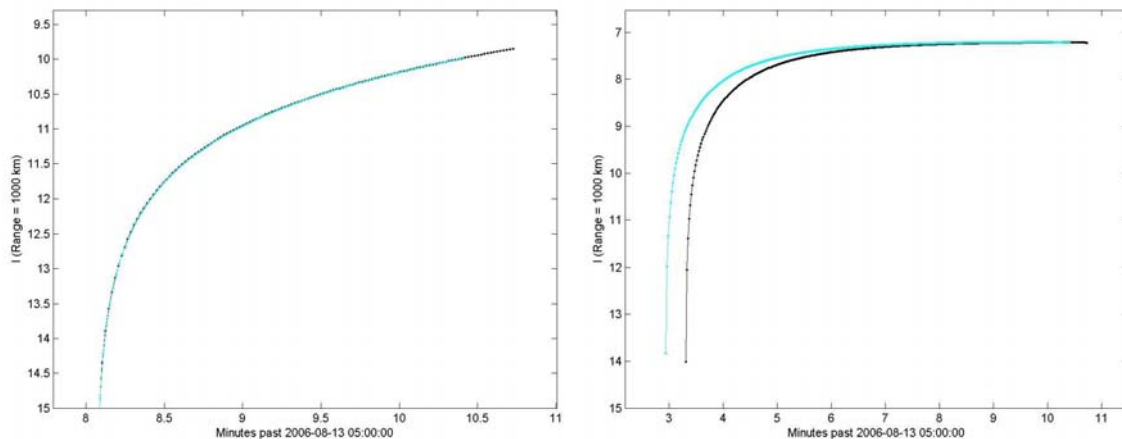


Figure 2. Simulated signatures of a single reflective facet in LEO as observed from Maui (black curves) and Kauai (blue curves). Each plot shows time on the x-axis and the brightness of reflected sunlight (in range-normalized stellar magnitudes) on the y-axis. The modeled facet has a Lambertian reflectivity of 30% with a surface area of 1 m^2 . The left panel shows an example where the facet becomes illuminated by sunlight during the pass, causing the brightness to increase simultaneously at both observing sites. The right panel shows an example where the facet becomes visible to the observers during the pass, causing the brightness to increase at slightly different times at the two sites.

4.4 Stabilized Object Attitude Tests

Another concept for a shape-independent attitude analysis method is that, for a rigid body, two independent measurements should have approximately equal brightnesses if the body-to-observer and body-to-Sun directions in the body frame of reference are both close to one another. This concept may be used to evaluate whether a set of attitude parameters are consistent with an ensemble of observations or not. For instance, if a hypothesized attitude model indicates that the body-to-observer and body-to-Sun directions for two observations are identically reproduced, but the measured fluxes are actually significantly different, then that hypothetical attitude model is most likely incorrect. A generalization of this concept involves performing this kind of comparison for all independent pairs of observations that have similar observation

and illumination directions. Simulation studies indicate this approach relies on large numbers of independent observations, and may require that glint events be filtered out of the observational data sets before analysis. Investigation and research continue to evaluate the utility of this concept.

5 ATTITUDE-INDEPENDENT SHAPE ANALYSIS

Preliminary research suggests that the distribution of satellite brightnesses observed as a function of solar phase angle (i.e., the Sun-satellite-observer angle) can be used as an attitude-independent indicator of object shape. The method entails comparing the phase-angle/brightness distribution of a well-observed object of unknown shape to that of a satellite with known shape, or to those simulated for a set of hypothesized shapes. In this context, “well-observed” indicates large numbers (>100) of independent observations of an object, ideally under multiple observing and illumination conditions spanning a large range of phase angles. The underlying assumption is that the large numbers of geometrically varied measurements comprise an essentially random set of observation and illumination conditions. In other words, the set of observations is assumed to be randomly drawn from a uniform distribution of satellite orientations relative to the observer and the source of illumination. This means that the observed pattern of brightness as a function of solar phase angle can be compared to that of a hypothesized shape, also randomly drawn from a uniform distribution of satellite orientations, to search a potential match. Figure 3 illustrates the concept, showing simulated phase-angle/brightness distributions for a uniform cube, tetrahedron, and cylinder in the form of scatter plots. Each panel shows the brightness (plotted on the y-axis) for a sample of 100,000 randomly selected viewing and illumination angles, plotted as a function of the solar phase angle (on the x-axis). Each point on the plots corresponds to a single observation. Figure 3 illustrates that these phase-angle/brightness distributions have a specific and distinct form for each simulated shape, and therefore can be used as an attitude-independent indicator of object shape.

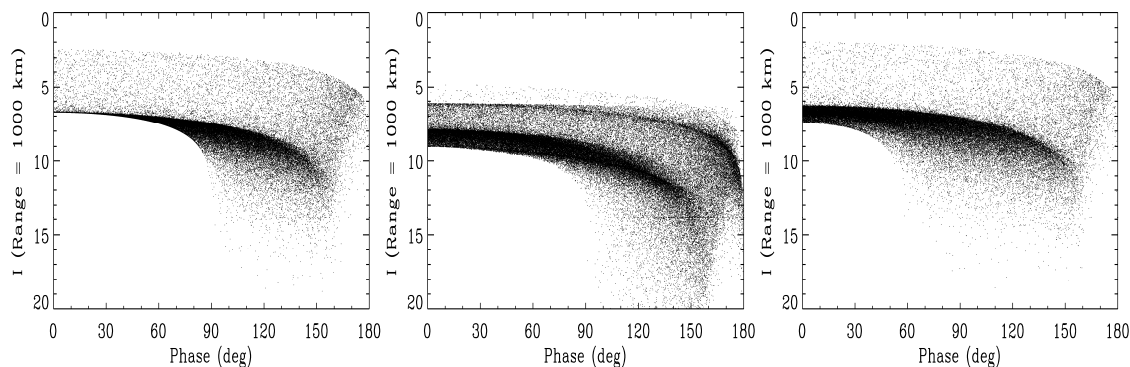


Figure 3. Simulated phase-angle/brightness distributions for a cube (left panel), a tetrahedron (middle panel), and a cylinder with a length-to-diameter ratio of 3:1 (right panel). The y-axis of each plot shows brightness in units of range-normalized stellar magnitudes vs. solar phase angle on the x-axes. Each simulated object was given 30% Lambertian and 30% specular albedos for all reflective surfaces and a size perfectly inscribable into a 1 m diameter sphere. Each scatter plot shows one point for a set of 100,000 randomly selected observation and illumination angles. These three two-dimensional distributions have distinctively different patterns that are characteristic of the object shape. Comparing such phase-angle/brightness distributions to those of a well-observed unknown satellite provides an attitude-independent means of evaluating the satellite’s shape.

In practice, this method requires the comparison of an observed two-dimensional phase-angle/brightness distribution to that simulated for a hypothesized shape. If the comparison is favorable (i.e., a statistical match) then the observed object could potentially be the hypothesized shape. Computational implementation requires an algorithm to compare two different two-dimensional scatter distributions and evaluate the probability of a statistical match, as given in reference [5]. During the comparison, care must be taken to generate distributions for the simulated shapes that have the same underlying phase-angle

frequency distribution as the observations, but that otherwise comprise a random set. Preliminary simulation studies indicate that the method works well for tumbling or un-stabilized objects as well as spin-stabilized satellites. However, the method often fails when applied to actively stabilized objects, because the underlying assumption that the measurements comprise a geometrically varied, essentially random set of observation and illumination conditions is not sufficiently satisfied.

6 CONCLUSIONS

Time-resolved radiometric measurements provide a means of constraining the attitude and/or shape of non-resolvable satellites. A detailed inversion of observational data entails the numerical solution of an integral-equation inversion problem, and requires solving for a large number of coupled attitude and shape parameters. By identifying that a set of facet albedo-area products can serve as a complete set of body parameters for convex objects, and that attitude parameters appear only in the kernel of the integral equation, the inversion process can be subdivided naturally into independent parts that can be calculated in parallel on a multi-node computer. The resultant facet-area distributions can be used to determine or at least constrain the shape of the observed satellites. Preliminary research indicates that separating the attitude and body parameter determination analyses more completely produces even more computational efficiency. For instance, the shape-independent synodic/sidereal periodic analysis method developed to derive the attitude parameters of spinning asteroids has been shown to work very efficiently for man-made satellites as well. Other shape-independent methods of constraining attitude, such as glint-timing and single-facet analysis, show promise especially for slowly-spinning or stabilized objects. Finally, comparing the phase-angle brightness distributions for well-observed objects to those expected for known shapes provides an attitude-independent means of constraining the shapes of non-resolved satellites.

7 REFERENCES

1. Magnusson, P. et. al., "Determination of Pole Orientations and Shapes of Asteroids," in *Asteroids II* (edited by R. Binzel et. al.) pp. 66–97, University of Arizona Press, Tucson AZ, 1989.
2. Kaasalainen, M. and Torppa, J., "Optimization Methods for Asteroid Lightcurve Inversion I. Shape Determination," *Icarus*, Vol. 153, pp. 24–36, 2001.
3. Kaasalainen, M. et. al., "Optimization Methods for Asteroid Lightcurve Inversion II. The Complete Inverse Problem," *Icarus*, Vol. 153, pp. 37–51, 2001.
4. Magnusson, P., "Distribution of Spin Axes and Senses of Rotation for 20 Large Asteroids," *Icarus*, Vol. 68, pp. 1–39, 1986.
5. Press, W. et. al., "Numerical Recipes in FORTRAN: The Art of Scientific Computing" (2nd Edition), Cambridge University Press, New York NY, 1992.
6. Lawson, C. and Hanson, R., "Solving Least Squares Problems" Prentice-Hall, Inc., Englewood Cliffs NJ, 1974.
7. Calef, B., et. al., "Photometric Signature Inversion" in "Unconventional Imaging II" ed. Gamiz, V., *Proceedings of SPIE*, Vol. 6307, 63070E, 2006.
8. Scargle, J., "Studies in Astronomical Time Series Analysis II. Statistical Aspects of Spectral Analysis of Unevenly Spaced Data," *The Astrophysical Journal*, Vol. 263, pp. 834–53, 1982.
9. Larsson, S., "Parameter Estimation in Epoch Folding Analysis," *Astron. Astrophys. Supp. Ser.*, Vol. 117, pp. 197–201, 1996.
10. Hall D. et. al., "AMOS Observations of NASA's IMAGE Satellite," *The 2006 AMOS Technical Conference Proceedings*, Kihei, HI, 2006.

11. Payne, T. et. al., "SSA Analysis of GEOS Photometric Signature Classifications and Solar Panel Offsets" *The 2006 AMOS Technical Conference Proceedings*, Kihei, HI, 2006.